Journal of The Electrochemical Society, **154** (1) B20-B24 (2007)
0013-4651/2006/154(1)/B20/5/$20.00 © The Electrochemical Society

High-Performance Ultrathin Solid Oxide Fuel Cells for Low-Temperature Operation

Hong Huang,* Masafumi Nakamura, Peichen Su, Rainer Fasching, Yuji Saito, and Fritz B. Prinz**

Rapid Prototyping Laboratory, Department of Mechanical Engineering, Stanford University, Stanford, California 94305, USA

Thin-film solid oxide fuel cell (SOFC) structures containing electrolyte membranes 50–150 nm thick were fabricated with the help of sputtering, lithography, and etching. The submicrometer SOFCs were made of yttria-stabilized zirconia (YSZ) or YSZ/gadolinium-doped ceria composites electrolyte and 80 nm porous Pt as cathode and anode. The peak power densities were 200 and 400 mW/cm^2 at 350 and 400°C, respectively. The high power densities achieved are not only due to the reduction of electrolyte thickness but also to the high charge-transfer reaction rates at the interfaces between the nanoporous electrodes (cathode and/or anode) and the nanocrystalline thin electrolyte.
 [DOI: 10.1149/1.2372592]

Manuscript submitted May 8, 2006; revised manuscript received August 11, 2006. Available electronically November 6, 2006.

Fuel cells convert chemical energy directly into electrical energy with higher efficiency when compared to traditional heat expansion engines. Currently, two types of fuel cells, polymer electrolyte membrane fuel cells (PEMFCs) and solid oxide fuel cells (SOFCs), are the subject of intense study. To date, temperature constraints, high cost, and technological difficulties have limited both fuel cell types to a narrow range of practical applications. In this paper, we focus on a new class of SOFCs made of ultrathin oxide films, which promise to lower operating temperature while delivering high power density.

At present, the minimum thickness of solid oxide electrolytes that can be mass-produced is tens of micrometers. Due to low ionic conductivity in solid electrolytes such as yttria-stabilized zirconia (YSZ), SOFCs must be operated above 700°C. Such high operating temperatures require special materials for sealing and heat maintenance, resulting in significant design challenges and high cost. In addition, at temperatures above 700°C reactions between material components may ultimately result in degradation of fuel cell performance. High operating temperatures restrict today's SOFCs to stationary applications only.[1,2] Currently, new materials and concepts are sought to reduce SOFC operating temperatures well below 700°C[3-6] so that they might be used for stand-by/supply power in micro and distributed combined heat and power (CHP) units as well as electric vehicles.[1] Moreover, SOFCs operating below 600–700°C allow the adoption of high-temperature (HT) gasket technology, thus permitting greater design flexibility in the choice of stack configurations.

The performance of a fuel cell is generally considered to be determined by activation loss originating from a limited rate of electrochemical charge-transfer reactions at cathode and anode and by ohmic loss stemming from the low ionic conductivity of the electrolyte membrane. At high current density, concentration loss, caused by limited diffusion of gases through the electrodes, is another key issue.[7,8] Assuming the concentration loss is small and the cathode activation loss is dominant, the voltage of a fuel cell (V) can be expressed as

$$V = emf - J \bullet ASR_e - \eta_{act} = emf - J \bullet ASR_e - \frac{RT}{\alpha nF} \ln \frac{J}{J_o} \quad [1]$$

where emf is the theoretical electromotive force, J is the current density, ASR_e is the area specific resistance of the electrolyte, R is the gas constant, F is the Faraday constant, J_o is the exchange current density, an indicator of the electrochemical charge-transfer reaction rate, and α is the corresponding transfer coefficient, which is typically between 0.2 and 0.3.[9] Among the best cathode materials ever reported are BSCF ($Ba_{0.5}Sr_{0.5}Co_{0.8}Fe_{0.2}O_{3-\delta}$)[10] and SSC ($Sm_{0.6}Sr_{0.4}CoO_{3-\delta}$)[11] with J_o of 10^{-3} to 10^{-2} A/cm^2 at 400°C, respectively. Correspondingly, ASR_e must be less than 0.2 Ω cm^2 to achieve sufficient P_{max} at low operating temperatures.

To date, solid-oxide electrolytes can be categorized into stabilized zirconia (e.g., YSZ, $Y_{0.16}Zr_{0.84}O_{2-\delta}$), doped $LaGaO_3$ (e.g., LSGM, $La_{0.9}Sr_{0.1}Ga_{0.8}Mg_{0.2}O_{3-\delta}$), doped ceria (e.g., GDC, $Gd_{0.2}Ce_{0.8}O_{2-\delta}$), and stabilized bismuth oxide (e.g., BVCO, $Bi_2V_{0.9}Cu_{0.1}O_{5.35}$).[1,2]

Among the four electrolyte materials, LSGM and GDC have higher ionic conductivities and hence they are frequently selected as electrolytes in intermediate temperature SOFC (IT-SOFC) structures. High peak power densities of 612 and 80 mW/cm^2 at 500 and 400°C, respectively, were recently reported by using 5 μm LSGM.[11] YSZ, which is known for its good stability but has comparatively low ionic conductivity, is generally excluded in IT-SOFCs. However, reducing the thickness of YSZ to below 200 nm we may achieve the desired ASR_e for IT-SOFCs. By employing submicrometer-thin highly conductive electrolytes such as LSGM or GDC, even higher power densities can be anticipated at low operating temperatures.

Fabrication of ultrathin SOFCs faces challenges regarding mechanical stability, electrical integrity (no shorts), and gas tightness (no leakage). Here, we present a process sequence consisting of thin film material deposition (sputtering), lithography, and material removal (etching). In addition, we report the *I-V* performances of the ultrathin SOFCs as well as the power densities measured in the temperature range between 300 to 400°C.

Experimental

Thin film deposition.— Sputtering is widely used in semiconductor processing. By adjusting the processing parameters, e.g., gas pressure, deposition power, temperature, and time, one can achieve different morphologies including fully dense and highly porous films. We fabricated porous Pt films for use as both cathode and anode by dc sputtering at 10 Pa Ar pressure, 100 W, and room temperature. Dense YSZ electrolyte films were deposited at 200°C by radio-frequency (rf) sputtering. The dc sputtering target was Pt and the rf sputtering target was $Y_{0.16}Zr_{0.84}O_{1.92}$. Both targets have 99.9% purity and are provided by Kurt Lesker Co. Before fuel cell characterization, the fuel cell structures were annealed at 400°C for 1 h in air. The morphologies of Pt and YSZ were examined with the help of scanning electron microscopy (SEM). The composition of yttrium and zirconium was analyzed using X-ray photoelectron spectroscopy (XPS).

Fabrication of submicrometer thin SOFCs.— Figure 1 illustrates the flow chart of the processing sequence we developed. A silicon wafer serves as support for the thin film SOFC. The wafer is

* Electrochemical Society Active Member.
** Electrochemical Society Student Member.

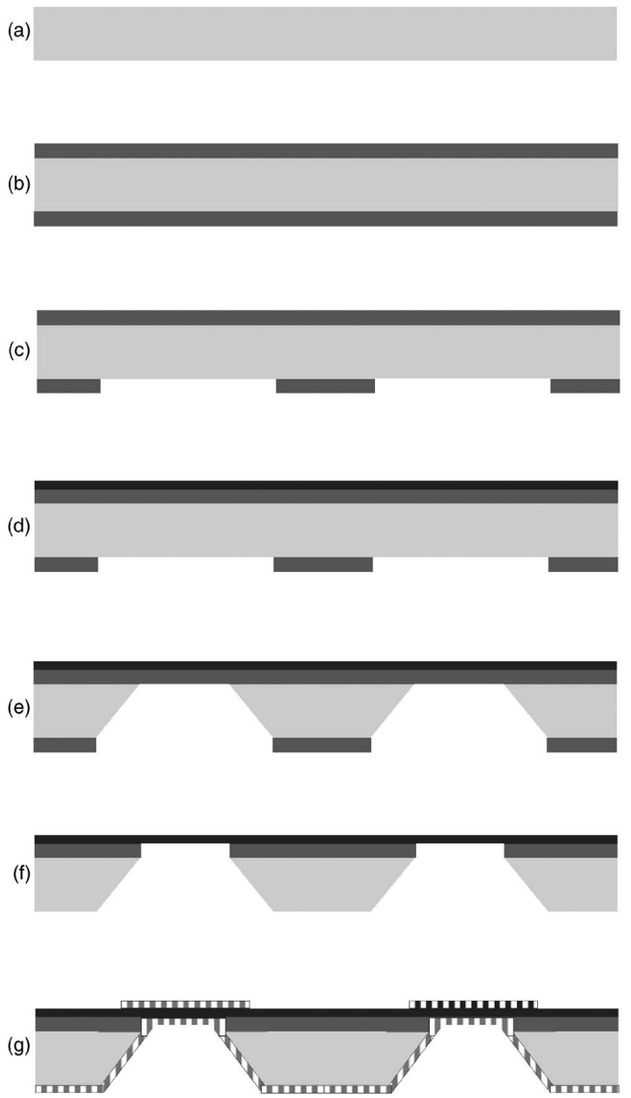

Figure 1. Flow chart of processing sequence for fabrication of ultrathin SOFCs.

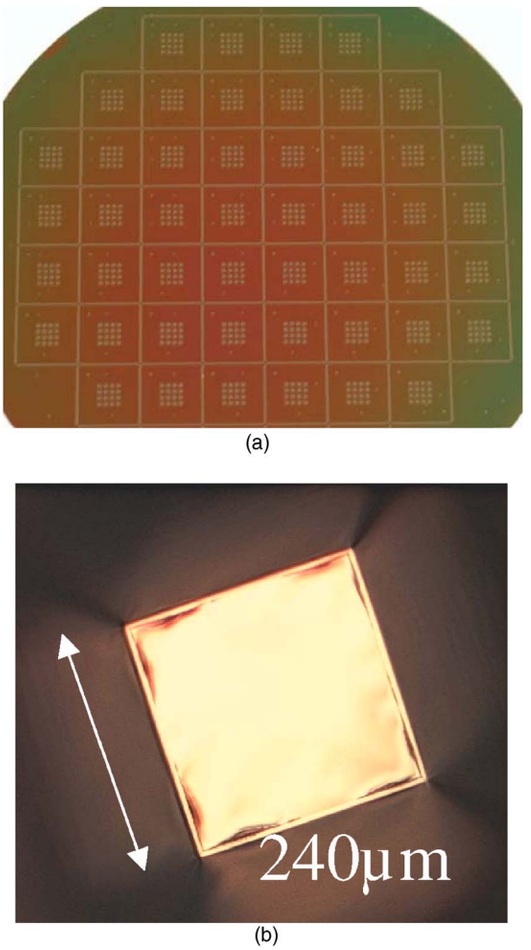

Figure 2. (Color online) Optical images of (a) the SOFC patterns on a 4 in. wafer and (b) free-standing individual fuel cell with maximum area.

4 in. in diameter, 375 μm thick, and double-polished (Fig. 1a). To prevent the electrical current from leaking and avoiding reaction between Si and YSZ, 500 nm thick low-stress silicon nitride was deposited on both sides of the wafer by low-pressure chemical vapor deposition (LPCVD) (Fig. 1b). Next, on one side (bottom) of the wafer, photoresist (3612 positive resist from Shipley Co.) was coated with designed mask, then exposed and developed followed by removal of the exposed silicon nitride by reactive ion etching (RIE) (Fig. 1c). Afterwards, the photoresist residue was stripped off by piranha etching. Then 50 nm 8YSZ was deposited on the other side (top) by rf sputtering at 200°C (Fig. 1d). The opened Si windows were etched with 30% KOH at temperatures of 85–90°C (Fig. 1e). Furthermore, silicon nitride in the window structure as well as that on top of Si was etched away by RIE (Fig. 1f). By using physical masks, 80 nm porous Pt films (cathode and anode) were patterned on both sides of YSZ. The fabricated structure was cut into 1×1 cm and subjected to fuel cell performance testing (Fig. 1g). The 4 in. wafer contains 832 individual fuel cells with different sizes, which can be characterized individually. The maximum area of the individual cells is 240×240 μm and the minimum area is 50×50 μm. Figure 2a and b exhibited optical images of the SOFC patterns on a 4 in. wafer and one free-standing individual cell.

SOFC performance characterization.— A testing chip (1 cm^2) containing 16 individual thin SOFCs was placed into the testing station, as shown in Fig. 3. The anode electrode was linked to a gold gasket with external electrical connection. The patterned cathode electrode was connected via a microprobe manipulator capable of measuring individual fuel cells. Constant chamber temperature was maintained with the help of a temperature regulator. The temperature in the vicinity of the tested individual fuel cells was also monitored. *I-V* data were collected with Solartron 1287 using both the galvanodynamic (scanning current) mode and the galvanostatic (constant current) mode. Electrochemical impedance spectra (EIS) were obtained with Solartron 1260/1287 in the frequency range of 50 kHz to 0.1 Hz with an ac amplitude of 20 mV. The EIS spectra were analyzed using Z-view software based on complex nonlinear least squares fitting.

Results and Discussion

Figure 4a presents the cross-sectional SEM of an ultrathin SOFC structure. The top light layer is the cathode Pt, and the bottom light layer is the anode Pt. In between, the darker layer represents the YSZ electrolyte. Both Pt cathode and anode layers were deposited by dc sputtering for 80 s. The deposition condition is 10 Pa Ar pressure, 100 W power, and room temperature. YSZ was deposited by rf sputtering for 100 min at 5 mTorr Ar pressure ($Ar:O_2$ ratio is 40:10)

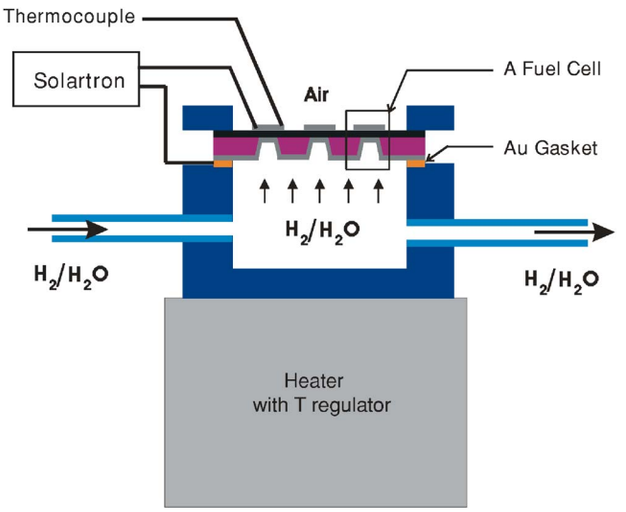

Figure 3. (Color online) Schematic of testing station for characterizing ultrathin SOFCs at low temperatures.

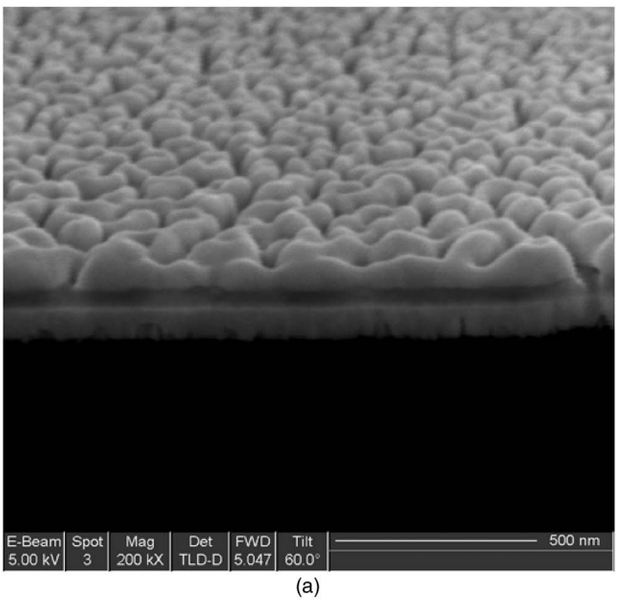

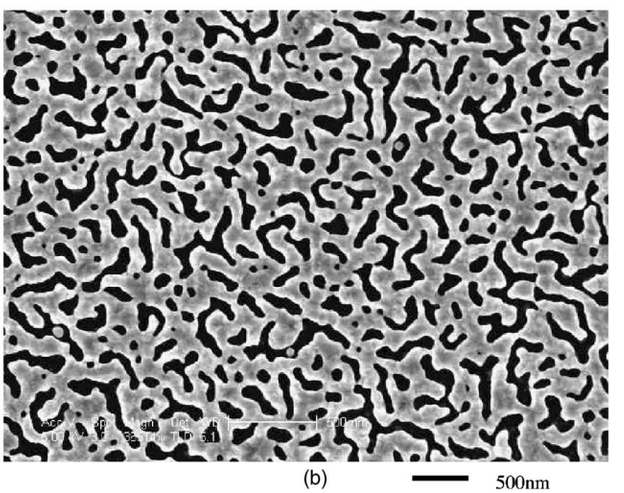

Figure 4. (Color online) SEM images of (a) cross-section of an ultrathin SOFC structure and (b) plane-view of Pt electrode morphology.

and 300 W. The temperature of the substrate was 200°C. Based on the SEM, the thicknesses of the Pt and YSZ layers were determined to be 80 and 50 nm. Hence, the deposition rates for Pt and YSZ are 1 nm/s and 0.5 nm/min, respectively. Figure 4b presents the plane-view of the Pt morphology. The pores in Pt electrode are in the range 100 nm and the porosity was estimated to 30–40%. Plane-view high resolution SEM imaging was also performed on YSZ film. The grain size of YSZ was observed to be 20–30 nm in average. XPS surface and depth analysis results indicated that Y to Zr ratio was close to 1:5 through the whole thickness.

The performances of the ultrathin SOFCs were evaluated using air as oxidant gas and dry/wet hydrogen (containing ~3% H_2O) as fuel gas. The SOFCs consisted of 50 nm thick YSZ electrolyte layers sandwiched between 80 nm thick porous Pt electrodes. The area of the tested SOFCs was confirmed to be 100 by 100 square micrometers based on SEM images. At 350°C open-circuit voltages (OCV) in the range 1.05 to 1.10 V were measured across the ultrathin SOFCs. The value was slightly lower than 1.16 V as predicted by Nernst equation due to slight gas leakages. Figure 5 presents the *I-V* curves of the thin-film SOFCs recorded at 350°C. The maximum power density was achieved 130 mW/cm^2 at 350°C out of the ultrathin SOFCs consisting of 50 nm YSZ electrolyte. To the best of our knowledge, such high power density at such low temperature has not yet been reported in the open literature. Thin SOFCs containing 100 and 150 nm thick YSZ were also fabricated by the same processes. The maximum power densities at 350°C were 85 and 60 mW/cm^2, respectively. No characteristic concentration loss was observed in the *I-V* curves suggesting that gas diffusion through the thin nanoporous Pt is sufficient within the limiting current. For comparison, an SOFC consisting of 50 μm thick YSZ ($Y_{0.16}Zr_{0.84}O_{1.92}$ in composition with average grain size of 600 nm, provided by Ceraflex Co.) and 80 nm thick Pt electrodes deposited at the same sputtering conditions was tested. The maximum power density was measured to be less than 1 mW/cm^2 at 350°C.

The high performance of the ultrathin SOFCs consisting of 50 nm thick nanocrystalline YSZ was not only due to the decrease of the ohmic resistance (decrease of ohmic loss) but also due to the high electrochemical charge-transfer reaction rate (decrease of activation loss). Figure 6 shows the electrochemical impedance spectra of an SOFC consisting of 50 nm YSZ recorded at 350°C. It is well known that the impedance arc in the high-frequency region corresponds to ionic conduction in the electrolyte, while the arc in the low-frequency region corresponds to the reaction processes at the electrode/electrolyte interface.[12] Accordingly, the ionic conductivity at 350°C of 50 nm YSZ is calculated to be 2×10^{-5} S/cm, consistent with 50 μm YSZ (2.5×10^{-5} S/cm) as well as previously reported data.[1] It is obvious from Fig. 6 that at open-circuit voltage the area specific electrode interfacial resistance (ASR_c) is around one order of magnitude higher than electrolyte resistance (ASR_e). This indicates that the major loss originated from electrode reaction process. The same behavior can be observed from the *I-V* curves, in which voltage drops dramatically at low current densities. On the other hand, ASR_c decreased significantly at 0.8 V. The electrode kinetics of the dominant process accelerated upon increasing the overpotential. It is frequently reported that cathode reaction kinetics are much slower than that of anode reaction in SOFCs.[5] These observations suggest to us that the ASR_c is mainly related to cathodic reaction. In other words, the cathode reaction dominates the activation loss.

Cathodic reactions were found much faster in highly ion-conductive electrolytes when the charge-transfer reaction at the TPB is the rate-determining step (RDS).[4,13] Tsai et al. reported that cathode resistance was decreased ten times by inserting yttria-doped ceria between YSZ and cathode.[14] To achieve a higher electrochemi-

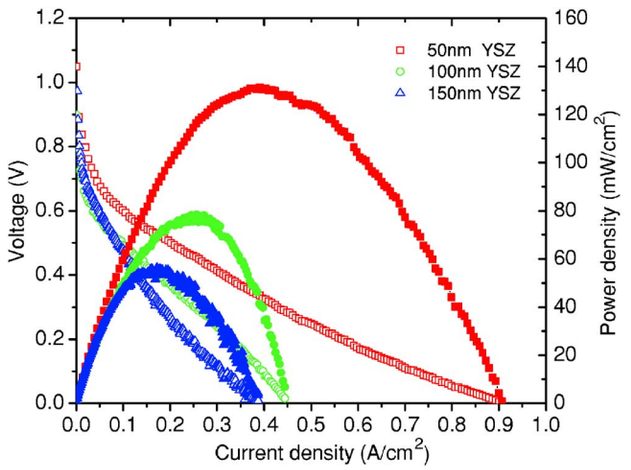

Figure 5. (Color online) *I-V* curves recorded at 350°C of micro-SOFC consisting of 50, 100, and 150 nm YSZ electrolytes, respectively. Both cathode and anode are 80 nm porous Pt.

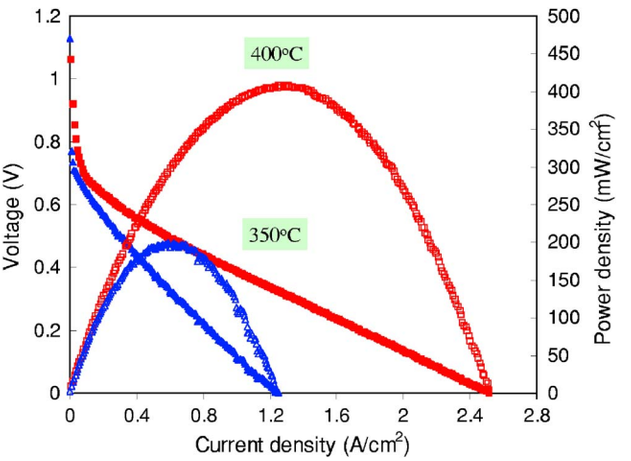

Figure 7. (Color online) Performances of nanothin SOFC consisting of 50 nm thick GDC interlayer between 80 nm thick cathode Pt, and 50 nm thick YSZ at 350 and 400°C. Solid symbols indicate voltage as a function of current density. Open symbols indicate power density as a function of current density.

cal charge-transfer reaction rate for improving fuel cell performance, we deposited nanothin gadolinia-doped ceria ($Gd_{0.1}Ce_{0.9}O_{2-\delta}$) as an active interlayer between the YSZ electrolyte and cathode. GDC was deposited on the YSZ by dc sputtering (the target was $Gd_{10}Ce_{90}$ in atomic ratio, 99.9% in purity, Kurt Lesker Co.) followed by oxidation in air at 600°C for 5 h. Figure 7 presents the performance of a thin-SOFC containing a 50 nm thick GDC interlayer between the YSZ and the cathode Pt. The *I-V* performances of the fuel cell were characterized in the temperature range of 300 to 400°C. The OCV was 1.10 V in the temperature range used. Although the total area specific resistance of electrolyte (ASR_e) was increased by 1–5% as a result of adding the 50 nm thick GDC interlayer, the maximum power density was increased to 200 mW/cm^2 at 350°C. At 400°C, the maximum power density reached 400 mW/cm^2. The peak power density at 300°C dropped down to 55 mW/cm^2.

In SOFCs the charge transfer at the cathode, the major source of the activation loss, is commonly expressed as

$$\frac{1}{2}O_2(\text{gas}) + 2e^-(\text{cathode}) \rightleftharpoons O^{2-}(\text{electrolyte}) \quad [2]$$

The actual reaction sequence is more complex. A general agreement exists that the oxygen reduction reaction undergoes four basic steps—oxygen molecule adsorption onto the catalyst surface, gas molecule dissociation into electroactive intermediate constituents such as atomic oxygen, formation of oxide-ions by charge transfer at the gas/electrode/electrolyte triple phase boundaries (TPB) for non-permeable electrode like Pt[9,15] and incorporation of oxide-ions into the electrolyte. The chain of reactants and products can then be modeled as

$$O_2(gas) \xrightarrow{\text{Pt}} O(\text{Pt}) \xrightarrow{e^-} O^{2-}(\text{TPB}) \xrightarrow{\text{oxide-ion vacancy}} O_O^x(\text{electrolyte}) \quad [3]$$

The precise sequence and location of charge-transfer reaction, as well as what mechanism is the RDS, is still under discussion as described in the review by Adler.[16] Meanwhile, according to theoretical analyses reported in previous reports,[17,18] small effective charge-transfer resistance, i.e., low activation overpotential, can be expected by using a thin cathode with fine microstructure and a highly ion-conductive electrolyte with small grain sizes. We also observed experimentally higher charge-transfer kinetics on the nanocrystalline YSZ than on YSZ with grain size of a few micrometers. Based on the previous models and our experimental results, the high electrochemical reaction rates we achieved are most likely related to the ultrathin highly porous Pt we deposited onto the nanocrystalline YSZ. We submit that in the vicinity of nanoporous Pt and nanocrystalline YSZ elevated levels of electroactive intermediate constituents such as atomic oxygen and oxide-ion vacancy may lead to improved electrochemical kinetics of oxygen reduction at the cathode. This hypothesis is also supported by the fact that oxygen exchange rates on the surface of nanocrystalline YSZ were found to be two orders of magnitude higher than that on the bulk YSZ,[19] suggesting better catalytic properties of oxygen dissociation on nanocrystalline YSZ surfaces. In addition, an extension of the charge-transfer reaction zone may occur in the vicinity of TPB due to enhanced diffusion on atomic scale surface discontinuities of the nanocrystalline electrolyte. Further investigations are in progress.

Good performances have been shown in HT-SOFCs by inserting doped ceria between YSZ and Sr-doped $LaCoO_3$ cathode. The doped ceria interlayer was considered to serve as a promoter for oxygen reduction reaction and a barrier to interaction between YSZ and cathode.[14,20] The former interpretation is more adaptable to our achievement in the thin SOFCs with GDC interlayer, as there is no reaction occurring between Pt cathode and YSZ electrolyte at the experimental conditions. Fast electrochemical reaction kinetics and hence, low activation loss, are attributed to elevated surface oxygen exchange rates and oxygen diffusivities on GDC.[21-23] It has been

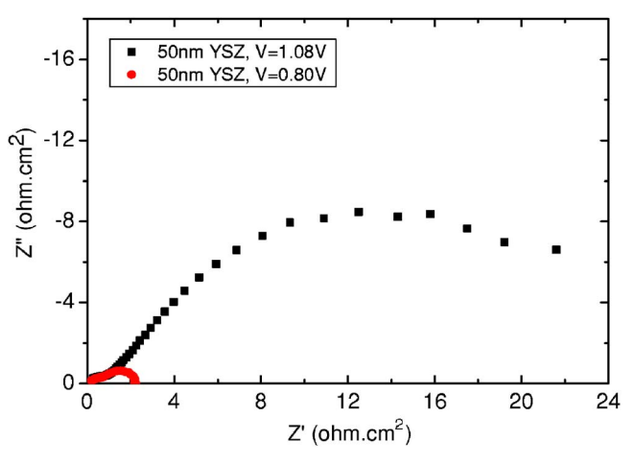

Figure 6. (Color online) Electrochemical impedance spectra of a micro-SOFC consisting of 50 nm YSZ recorded at OCV and 0.8 V across the fuel cell.

reported that the charge-transfer overpotential increases with decreasing ionic conductivity of the electrolyte,[13] suggesting a correlation between the charge-transfer reaction rate and local oxide-ion vacancy concentration and/or diffusivity. This is also corroborated with Tanner and Virkar's model,[17] as ionic conductivity of GDC is more than 10 times higher than YSZ. Moreover, we found, based on quantum simulations, that oxygen dissociation on doped ceria and the subsequent incorporation into surface vacancy sites is energetically more favorable relative to YSZ.[24] Because the GDC layer resides on the cathode side, the formation of Ce (III) due to the reduction by hydrogen, which may contribute to high electronic conductivity, is unlikely. Even in a reducing atmosphere, GDC can be transformed into a mixed conductor only at temperatures above 500°C.[23,25] However, Ce (III) residing on the surface of nano-GDC particles[26] cannot be excluded from playing a role in promoting the oxygen reduction reaction. Further investigations are required to understand details of the mechanism.

The results presented here are based on individual fuel cells with small areas. We are currently employing MEMS fabrication technologies to substantially increase the effective fuel cell area for high power output in the future.

Conclusions

We successfully fabricated ultrathin SOFCs by using thin film fabrication methods, including sputter deposition, lithography, and silicon etching techniques. By reducing the thickness of YSZ to submicrometers, *ASR* of electrolyte is significantly reduced. SOFCs consisting of 50, 100, and 150 nm thick YSZ electrolytes can be operated as low as 350°C with peak power density of 130, 80, and 60 mW/cm^2, respectively. Upon further improving the cathodic reaction kinetics by using GDC active interlayer, the peak power density value reached 400 and 200 mW/cm^2 at 400 and 350°C, respectively, which, to the best of our knowledge, are the highest power densities at temperatures below 400°C ever reported in the open literature. It is believed that by using highly ion-conductive electrolyte materials such as LSGM or GDC, cathode materials including BSCF and SSC, and novel electrode/electrolyte composites, further performance improvements may be possible. The present SOFC architecture may open new applications for SOFCs in transportation and portable microelectronic devices.

Stanford University assisted in meeting the publication costs of this article.

References

1. B. C. H. Steele and A. Heinzel, *Nature (London)*, **414**, 345 (2001).
2. B. P. Brandon, S. Skinner, and B. C. H. Steele, *Annu. Rev. Mater. Res.*, **33**, 183 (2003).
3. J. M. Ralph, A. C. Schoeler, and M. Krumpelt, *J. Mater. Sci.*, **36**, 1161 (2001).
4. T. Hibino, A. Hashimoto, T. Inoue, J. Tokuno, S. Yoshina, and M. Sano, *Science*, **288**, 2031 (2000).
5. S. Souza, S. J. Visco, and L. C. De Jonghe, *Solid State Ionics*, **98**, 57 (1997).
6. X. Chen, N. J. Wu, L. Smith, and A. Ignatiev, *Appl. Phys. Lett.*, **84**, 2700 (2004).
7. L. Carrette, K. A. Friedlich, and U. Stimming, *Fuel Cells*, **1**, 1 (2001).
8. R. O'Hayre, S. Cha, W. Colella, and F. B. Prinz, *Fuel Cell Fundamentals*, John Wiley and Sons, New York (2006).
9. M. Godickemeier, K. Sasaki, L. Gauckler, and I. Riess, *J. Electrochem. Soc.*, **144**, 1635 (1997).
10. Z. Shao and S. M. Haile, *Nature (London)*, **431**, 170 (2004).
11. J. Yan, M. Matsushige, M. Enoki, and T. Ishihara, *Electrochem. Solid-State Lett.*, **8**, A389 (2005).
12. E. Barsoukov and J. R. Macdonald, *Impedance Spectroscopy: Theory, Experiment, and Applications*, 2nd ed., John Wiley and Sons, New York (2005).
13. H. Uchida, M. Yoshida, and M. Watanabe, *J. Phys. Chem.*, **99**, 3282 (1995).
14. T. Tsai and S. A. Barnett, *Solid State Ionics*, **98**, 191 (1997).
15. J. Van Herle, A. J. McEnvoy, and K. T. Ravindranathan, *Electrochim. Acta*, **39**, 1675 (1994).
16. S. B. Adler, *Chem. Rev. (Washington, D.C.)*, **104**, 4791 (2004).
17. C. W. Tanner, K. Z. Fung, and A. V. Virkar, *J. Electrochem. Soc.*, **144**, 21 (1997).
18. S. H. Chan, X. J. Chen, and K. A. Khor, *J. Electrochem. Soc.*, **151**, A164 (2004).
19. G. Knoner, K. Reimann, R. Rower, U. Sodervall, and H. E. Schaofer, *Proc. Natl. Acad. Sci. U.S.A.*, **100**, 3870 (2003).
20. S. P. Simner, J. F. Bonnett, N. L. Canfield, K. D. Meinhardt, V. L. Sprenkle, and J. W. Stevenson, *Electrochem. Solid-State Lett.*, **7**, A173 (2002).
21. A. J. McEnvoy, *Solid State Ionics*, **132**, 159 (2000).
22. B. C. H. Steele, *Solid State Ionics*, **75**, 157 (1995).
23. H. Inada and T. Tagawa, *Solid State Ionics*, **83**, 1 (1996).
24. T. Holme and F. B. Prinz, Private communication.
25. M. Mogensen, N. M. Sammes, and G. A. Tompsett, *Solid State Ionics*, **129**, 63 (2000).
26. L. Wu, H. J. Wiesmann, A. R. Moodenbaugh, R. F. Klie, Y. Zhu, D. O. Welch, and M. Suenaga, *Phys. Rev. B*, **69**, 125415 (2004).